Semiclassical Analysis of Quantum Mechanical Calculations of Rotationally Inelastic Collisions of He and Ar with NaK[†]

Ashley Towne
Advisor: A. P. Hickman

July 31, 2015

Abstract

Recent quantum mechanical calculations and laboratory experiments at Lehigh University have provided detailed information about rotationally inelastic collisions of He and Ar with NaK in a cell at thermal energies. The purpose of this project was to develop a semiclassical model for these collisions based on the well-known vector model. In the quantum mechanical theory, Grawert coefficients $B_\lambda(j, j')$ (where λ is an integer) give the probability that a discrete amount $\lambda\hbar$ of angular momentum is transferred from the projectile to the target in a transition between rotational levels j and j'. Derouard showed that one can develop a semiclassical model by transforming from λ to the continuous variable α, the angle between initial and final angular momentum vectors $\boldsymbol{j}$ and $\boldsymbol{j'}$. In the present work we invoked the vector model, which relates the polar angle θ of the angular momentum vector to the azimuthal quantum number m, and showed that the distribution $P(\theta, \theta') \sin\theta'$ of final polar angles θ' could be expressed as a convolution of the semiclassical Grawert coefficient $B(j, j'; \cos\alpha)$. Using this expression we calculated the expected distribution of values of $\Delta\theta = \theta' - \theta$ and compared it with the quantum mechanical result. The semiclassical model agreed very well with the quantum mechanical theory, especially when the quantum number j was large. The distribution of projections of j onto the z axis before and after collision (in a transition $jm \to j'm'$) demonstrated (as others have also noticed) that m changes in such a way that θ tends to be preserved. The semiclassical model also predicts the propensity for collision-induced changes in j to be even numbers, in agreement with quantum mechanical theory and experiment.

[†]Work supported by NSF grants PHY-1359195, PHY-0968898, and PHY-1403060.

Contents

1 Introduction

NaK, like any molecule, can vibrate and rotate and can be described by the quantum numbers that characterize these vibrational and rotational states. Upon collision with a perturbing atom, such as helium or argon, these quantum numbers can change, signifying a transition from one state to another. This project is primarily concerned with collisions where the vibrational state is conserved, but the rotational state changes, as Eq. 1 specifies.

$$\begin{aligned} \mathrm{He} + \mathrm{NaK}(v, j, m) &\rightarrow \mathrm{He} + \mathrm{NaK}(v, j', m') \\ \mathrm{Ar} + \mathrm{NaK}(v, j, m) &\rightarrow \mathrm{Ar} + \mathrm{NaK}(v, j', m') \end{aligned} \tag{1}$$

Specifically, the purpose of this investigation was to explore the physical interpretation of how the quantum numbers that describe angular momentum change during collision. The vector model was extended to describe not only one angular momentum state but a transition between two states.

In addition to its rotational and vibrational states, NaK can also be described by its electronic state, which the set of potential curves express. A set of NaK's potential curves, calculated by Magnier [1], can be seen in Figure 1. The potential curves represent energy as a function of internuclear separation between sodium and potassium. Both experimental and theoretical investigations choose one potential curve to study, specifying the electronic energy level at which the collisions in question take place.

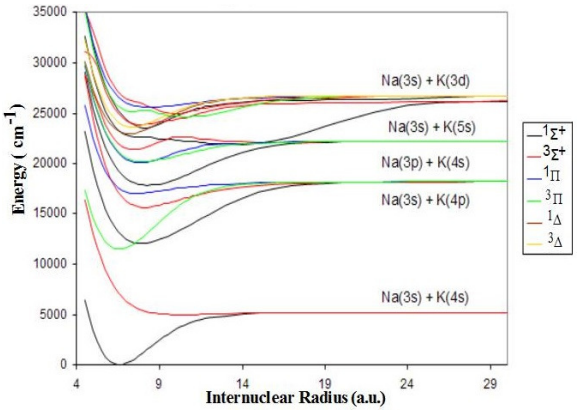

Figure 1: Potential curves for NaK. The electronic state of interest for this work is the first excited $^1\Sigma^+$ state.

2 Background

2.1 Experimental Measurements

At Lehigh University, the experimental and theoretical groups have worked together to investigate the collisions in question. Recent experiments have studied NaK+He, NaK+Ar, NaK+K, NaCs+He, and NaCs+Ar collisions [2, 3]. Related theory has examined NaK+He and NaK+Ar collisions as well as trends in the vector model and its semiclassical approximations in [4, 5, 6]. Currently at Lehigh, Professor Huennekens leads the experimental group, and Professor Hickman leads the theory group.

Professor Huennekens' group has measured the rate constants k of transitions, which are related to the cross sections [7]. The rate constants are proportional to the thermal average of the product of the cross section and velocity, which can be approximated as the cross sections times the average velocity:

$$k = \langle \sigma v \rangle \tag{2}$$

The cross section is proportional to the likelihood that a particular transition will occur from one j state to another. The rate constants average over all values of the quantum number m.

The experimental group has also measured the fraction of orientation that is preserved throughout the collisions [7]. Collisions tend to be randomizing processes, so studying the extent to which orientation is preserved gives information about the extend to which a collision changes the direction of the angular momentum vector. In a cell environment, such as the system that the experimental group studies, the angular momenta initially point in all directions and the average value of m, or $\langle m \rangle$ is zero; in other words, the orientation is zero. In order to measure the change in orientation, the initial orientation must be nonzero. The orientation is proportional to the expectation value of m for a particular j state:

$$O^j = \frac{\langle m \rangle}{\sqrt{j(j+1)}} \tag{3}$$

Physically, it is the extent to which all angular momenta are oriented, or point in the same direction.

2.2 Vector Model

The orientation is related to the geometric relationship between m and $\boldsymbol{j}$ in the vector model. The vector model provides a way of understanding

angular momentum, where $\boldsymbol{j}$ is the angular momentum vector, and what it means for all angular momenta to point in the same direction. As seen in Figure 2, the quantum number m is the projection of $\boldsymbol{j}$ onto the z axis: $\boldsymbol{j}$ can

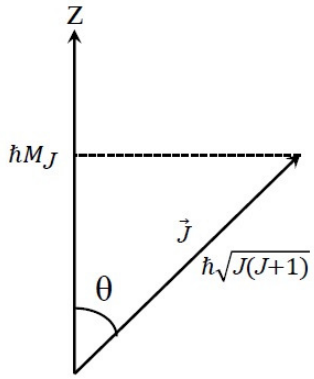

Figure 2: Vector model of angular momentum

precess around the z axis at a constant θ without changing its magnitude or the magnitude of m, as stated by Eq. 4:

$$\cos\theta = \frac{m}{\sqrt{j(j+1)}} \tag{4}$$

The expectation value of the $\cos\theta$ is the orientation, as Eq. 3 stated.

2.3 Experimental Procedure

In order to ensure a nonzero orientation for the initial state of the system, the experimental group excites the system from the ground state to a higher potential, the $A^1\Sigma^+$ state. These states are selected potential curves from Figure 1, shown in more detail in Figure 3. The bottom curve is the ground state $X^1\Sigma^+$. A circularly polarized pump laser populates the vibrational and rotational states in the $A^1\Sigma^+$ state. After the collisions, the probe laser is swept across a range of frequencies to measure the orientation, exciting the system to the top curve, the $3^1\Pi$ state.

Polarized light always has selection rules for the states it populates, and the circularly polarized pump laser's selection rule is that $\Delta m = +1$. The $A^1\Sigma^+$ state has a preferential population of large m. This can be seen in Figure 4, where each row represents the m states available for the different potentials. The arrows represent transitions between these states that are possible due to laser excitation.

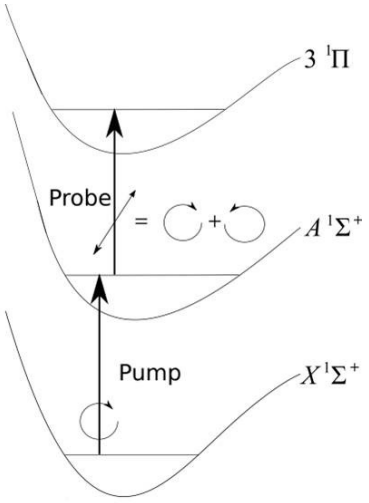

Figure 3: Selected potentials of NaK: $3^1\Pi$ (top), $A^1\Sigma^+$ (middle), $X^1\Sigma^+$ (bottom)

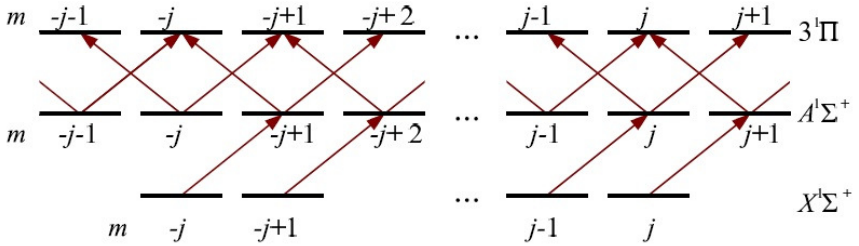

Figure 4: Possible m states and transitions: $3^1\Pi$ (top), $A^1\Sigma^+$ (middle), $X^1\Sigma^+$ (bottom)

The probe laser is linearly polarized; linear polarization can be expressed as a superposition of left and right circularly polarized light. Because of the initial nonzero orientation of the system, the opposing circular polarizations interact with the system differentially. The left circular polarization will see a different set of states that are available for transition than right circular polarization. After interacting with the sample, the remaining superposition of both polarizations of light is passed through a linear polarizer perpendicular to the initial polarization. If the laser's total polarization is unchanged, that is if transitions are not detected, no signal will pass through the polarizer. However, because the left and right circular polarizations are absorbed differently, the superposition after interacting with the system is no longer

perfectly linear but rather elliptically polarized. Therefore, whatever signal is detected after the polarizer is proportional to the final orientation [2].

2.4 Previous Results

A key feature of recent experimental results is the propensity for the change in j to be even numbers. Recent theoretical calculations are in good agreement with this result, as shown in Figure 5. Note that the theoretical rate constants were determined using the approximation that the rate constant is proportional to the cross section times the average velocity, as seen in Eq. 5.

$$k \approx \sigma \overline{v} \tag{5}$$

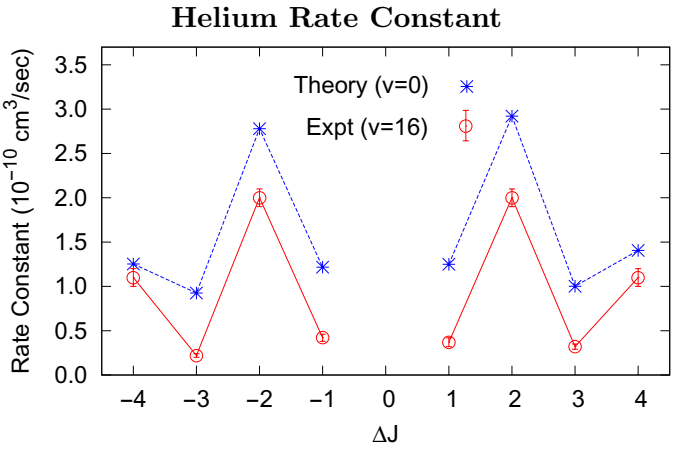

Figure 5: Experimental [2] and theoretical [4] rate constants

It was originally thought that this propensity was related to the strict selection rule for homonuclear diatomic molecules where no odd Δj transitions are allowed at all. Sodium and potassium are in the same column of the periodic table, so it was thought that perhaps NaK was approximately homonuclear, which would explain the propensity observed when the perturbing atom is the noble gas helium or argon [2]. However, it has been demonstrated that the propensity for an even Δj depends on the collision partner, whereas behavior of an approximately homonuclear molecule should depend solely on the molecule. Some experimental results for NaK in certain states in a collision with potassium show no propensity for even Δj at all [3].

Unfortunately, theory has large computational requirements, and it is computationally too expensive to model NaK+K to confirm. However, it can be concluded that some mechanism other than approximate homonuclear behavior is affecting the Δj propensity in both experiment and theory.

3 Analysis of Tipping Angle Distribution B

3.1 Goals: Physical Interpretations

The large calculations for the theoretical analysis are used to calculate $B_\lambda(j, j')$ values, which are the discrete probabilities for transferring a specific amount of angular momentum (λ) to the NaK molecule in the transition from j to j'. These calculations were done prior to the beginning of the summer.

The goal of this summer's project was to gain a deeper physical understanding of the angular momentum transitions. The vector model facilitated understanding the relationship between $\boldsymbol{j}$, $\boldsymbol{j'}$, λ, and α. λ gives the discrete value of angular momentum transferred in the collision, or the distance between the tip of the $\boldsymbol{j}$ vector and the tip of the $\boldsymbol{j'}$ vector in the vector model. Quantum mechanically, there are a finite number of discrete λ values for a given $j \to j'$ transition. α is the angle between $\boldsymbol{j}$ and $\boldsymbol{j'}$ and is likewise discrete.

3.2 Quantum Mechanical Model

$B_\lambda(j, j')$ values are used to calculate the cross section of interaction; the latter is given by Eq. 6. $B_\lambda(j, j')$'s are discrete probabilities for a particular transfer of angular momentum λ.

$$\sigma(j \to j') = \frac{\pi}{(2j+1)k_j^2} \sum_{\lambda=|j-j'|}^{j+j'} (2\lambda+1) B_\lambda(j, j') \tag{6}$$

λ can best be described by extending the vector model to include two different $\boldsymbol{j}$ vectors rather than one, such that $\boldsymbol{j}$ is the initial angular momentum vector and $\boldsymbol{j'}$ is the final angular momentum vector. See Figure 6. λ is the distance between the tip of the $\boldsymbol{j}$ and $\boldsymbol{j'}$ vectors. Since $\boldsymbol{j}$ and $\boldsymbol{j'}$ can precess about the z axis as well as have an altitude of any allowed θ, λ can range in magnitude from the difference in the two $\boldsymbol{j}$ vectors to their sum. Physically, λ represents how much angular momentum was transferred in the collision. The angle α is the angle between $\boldsymbol{j}$ and $\boldsymbol{j'}$. This parameter is

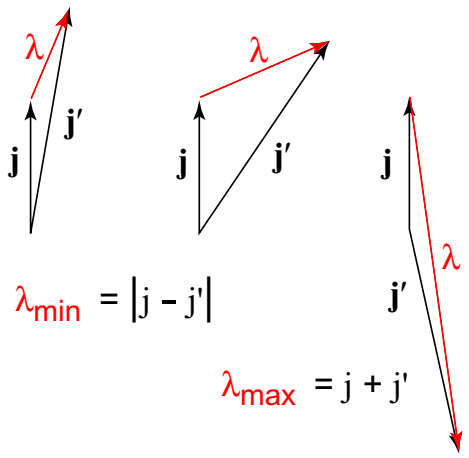

Figure 6: λ's relation to $\boldsymbol{j}$, $\boldsymbol{j'}$, and α.

called the tipping angle. It is a measure of how much the collision "tipped" $\boldsymbol{j'}$ from $\boldsymbol{j}$.

3.3 Semiclassical Model

In order to find a more intuitive physical interpretation, a semiclassical model was used, based on ideas introduced by Derouard [6]. Using the law of cosines and the relationship shown in Figure 6, the tipping angle can be related to the discrete amount of angular momentum, as in Eq. 7. By allowing α to be a continuous variable and making the appropriate substitutions, the discrete sum over λ in Eq. 6 can be transformed to an integral over α, as in Eq. 8.

$$\lambda(\lambda+1) = j(j+1) + j'(j'+1) - 2\sqrt{j(j+1)j'(j'+1)}\cos\alpha \tag{7}$$

$$\sigma(j \to j') = \frac{\pi(j'+1/2)}{k_j^2}\int_0^\pi B(j,j',\cos\alpha)\sin\alpha d\alpha \tag{8}$$

$B(j,j',\cos\alpha)$ is related to $B_\lambda(j,j')$. Rather than a discrete probability, it is the continuous distribution of tipping angles.

3.4 Results of B analysis

Plotting the $B_\lambda(j,j')$ and $B(j,j',\cos\alpha)$ values against the tipping angle α shows which α's are most likely. Larger B values correspond to a more likely tipping angle. Plotting B vs. α shows which tipping angles are most likely.

As B tends to be larger for smaller α, the most probable tipping angles are small. Helium and argon display similar overall behaviors. Compare Figure 7a to Figure 7b.

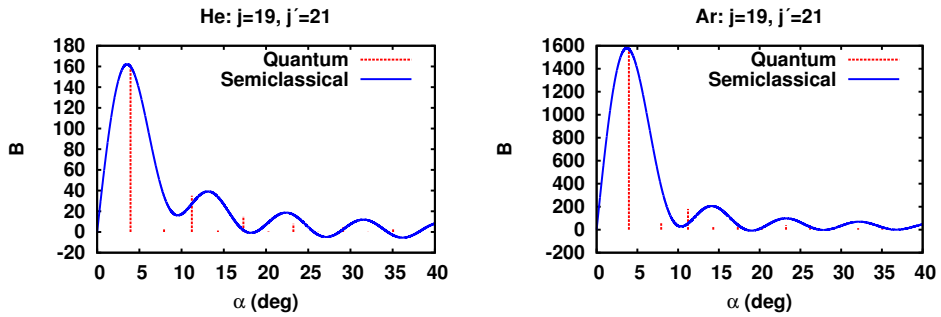

(a) Helium (b) Argon

Figure 7: Comparison of discrete values $(2\lambda+1)B_\lambda(j,j')$ (shown as vertical lines) with the continuous function $B(j,j',\cos\alpha)$

Both collisions favor small tipping angles. Argon's B values have larger magnitudes than helium's B values, so argon's cross sections also tend to be larger. Helium and argon tend to have similar rate constants, but argon has lower average velocities at a given energy. These trends are consistent with Eq. 2.

3.5 Conclusions for B Analysis

The quantum mechanical and semiclassical models agree rather well. Both exhibit oscillatory behavior as a function of angle, and the relative magnitudes between peaks and troughs tend to have similar trends. For simplicity, the following conclusions apply to both models.

Helium's B values were larger for even Δj transitions than for odd Δj transitions, which was expected due to the propensity for even Δj. Argon showed no such propensity in its B values. This is not entirely unexpected; in experiment, the propensity in collisions with helium is much stronger than it is for argon. Theoretical calculations successfully demonstrate the propensity for helium, although the theoretical propensity is much smaller than what has been observed in experiment. It is possible that, because argon's propensity is so much smaller than helium's, and because the theoretical model attenuates the propensity with respect to experiment, the propensity is too small for theory to detect at this point. However, a re-

fined potential curve has recently been calculated [8], which may improve the theoretical calculations.

As $\overline{j}$ increases, the expected tipping angle decreases. As Δj increases, so does the average α. These conclusions for helium were determined by treating even Δj separately from odd Δj. For example, as Δj increases, the expected α for each successive even Δj is larger than the last. However, α for even Δj tends to be smaller than for odd Δj when the two Δj's are not far apart.

Overall, α tends to be small, especially for more likely transitions. When the tipping angle is large, the transitions are less likely; likewise the large tipping angles contribute less to the total number of transitions than smaller tipping angles.

4 Cross Section Analysis

4.1 $\Delta\theta$: Vector Model

To analyze the cross sections, Eq. 6 and 8 were evaluated as a sum over λ for the quantum mechanical model and as an integral over α for the semiclassical model. Finding the cross section averages over all possible collisions. Recall the geometric relationship between m, $\boldsymbol{j}$, and θ from Eq. 4.

$$\cos\theta = \frac{m}{\sqrt{j(j+1)}} \tag{4}$$

$\Delta\theta$ is defined as:

$$\Delta\theta \equiv \theta' - \theta \tag{9}$$

Note that $\Delta\theta$ need not be the same as α, the tipping angle. Solving for θ from Eq. 4 and plugging it into Eq. 9 gives the relation in Eq. 10.

$$\Delta\theta = \arccos\left(\frac{m'}{\sqrt{j'(j'+1)}}\right) - \arccos\left(\frac{m}{\sqrt{j(j+1)}}\right) \tag{10}$$

The purpose of this analysis is to examine the cross sectional distribution against $\Delta\theta$. The difference between α and $\Delta\theta$ must not be overlooked. α and $\Delta\theta$ are only equivalent if $\boldsymbol{j}$ and $\boldsymbol{j'}$ are coplanar both with each other and the z axis, as appears to be the case in Figure 8a.

It is much more common, however, for $\boldsymbol{j}$ and $\boldsymbol{j'}$ to precess about the z axis. For a particular α and initial θ, then, the $\boldsymbol{j'}$ vector can point anywhere on the circle in Figure 8b.

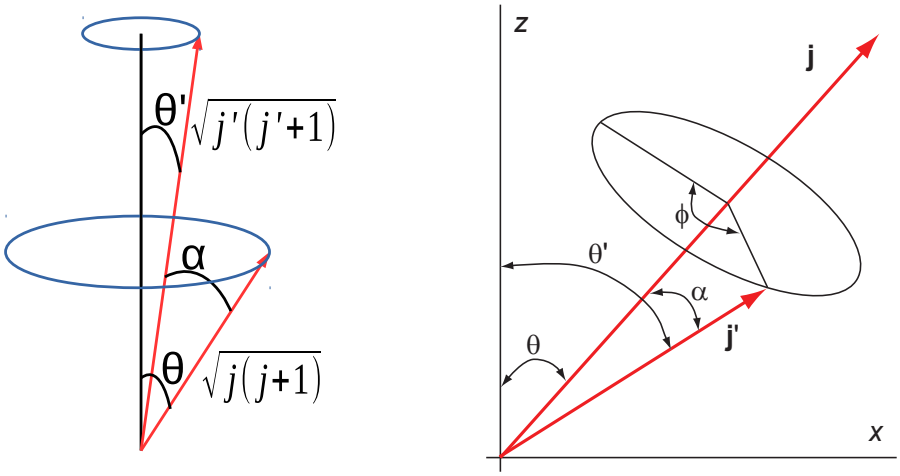

(a) $\boldsymbol{j}$ and $\boldsymbol{j'}$ appear to be coplanar with each other and the z axis, so $\alpha = \Delta\theta$

(b) Possible $\boldsymbol{j'}$ vectors given an initial $\boldsymbol{j}$ and α

Figure 8: Vector model expansion

If the azimuthal angle ϕ in Figure 8b is a continuous variable, there are exactly two possible $\boldsymbol{j'}$ vectors (and thus two θ' values) where $\Delta\theta$ is exactly zero. In this case, $\boldsymbol{j}$ will not point in the same direction as $\boldsymbol{j'}$; $\boldsymbol{j}$ and $\boldsymbol{j'}$ will never be collinear for a nonzero α.

4.2 Quantum Mechanical Analysis

For the quantum mechanical model, $\Delta\theta$ was computed from the initial and final states using j, j', m, and m' for all possible $m \rightarrow m'$ transitions, as in Eq. 10. The cross sections associated with each $\Delta\theta$ were put into a histogram using ranges of $\Delta\theta$. A convolution of the histogram values with a Gaussian transforms the discrete probabilities into a distribution for comparison with the semiclassical model. This process broadens the discrete values, which are essentially delta functions ($\delta(\Delta\theta)$), into a distribution that could be compared with the semiclassical model. Only a finite number of discrete values of ϕ (the azimuthal angle in Figure 8b) are allowed due to quantum mechanics. α, j, j', m, and m' likewise have a finite number of allowed values.

4.3 Semiclassical Analysis

The semiclassical model allows ϕ to be a continuous variable. Given an initial θ, for all azimuthal ϕ, a distribution of θ' can be determined. The final result is Eq. 11 which represents the θ' distribution as a convolution of the tipping angle distribution B.

$$P(\theta, \theta') \sin \theta' = \frac{\sin \theta}{\pi} \int_{-1}^{1} \frac{B(j, j'; \cos\theta \cos\theta' + y \sin\theta \sin\theta')}{\sqrt{1 - y^2}} dy \qquad (11)$$

A complete derivation can be found in Professor Hickman's work [9], but suffice it to say that the distribution integrates over all values of alpha allowed by the geometry, and that the form is convenient for evaluation by Gauss-Chebyshev quadrature of the first kind. The range of integration is such that $\cos(\theta + \theta') < \cos\alpha < \cos(\theta - \theta')$.

4.4 Results: $\theta \rightarrow \theta'$

The semiclassical distribution for a few chosen θ values can be seen in Figure 9. For each distribution, the peak is centered where $\theta = \theta'$, or, equivalently, where $\Delta\theta = 0$. The orientation tends to be conserved, according to the semiclassical model. The next section will show that this result is also approximately valid quantum mechanically.

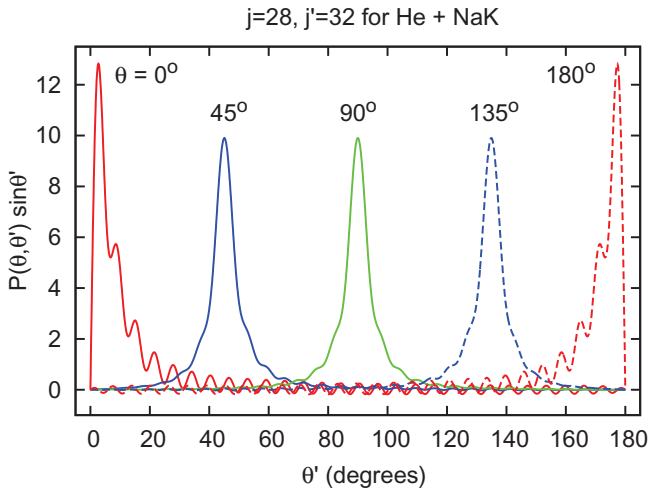

Figure 9: Distribution of θ' for $\theta = 0^o$, $\theta = 45^o$, $\theta = 90^o$, $\theta = 135^o$, $\theta = 180^o$

4.5 Results: Cross Section vs. $\Delta\theta$

We averaged the quantum mechanical results over all possible $jm \to j'm'$ transitions, calculating $\Delta\theta$ for each transition and weighting each $\Delta\theta$ by the corresponding cross section. This procedure enabled us to construct the histogram as shown in Figure 10, which compares the semiclassical and quantum mechanical results for $j \to j' = 28 \to 32$. The quantum mechanical curve is difficult to see in this figure because the two models agree very well. However, the peak in the graph is evidently at $\Delta\theta = 0$, which is as expected.

As $\overline{j}$ increases, however, the agreement declines. The disagreement depends both on the average value of j and the value of Δj. It appears that the smaller value of j must not be too small. When the smaller value of j is small, the disagreement is much greater. As fewer j states can be averaged over, the behavior looks less classical and more quantum mechanical. See Figure 11. For all $\overline{j}$, though, the most probable transitions are near small

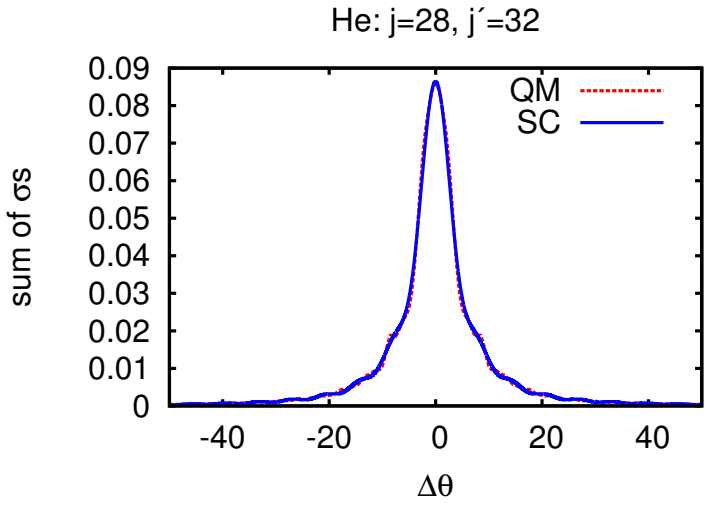

Figure 10: Cross sectional distribution vs. $\Delta\theta$, averaged over all collisions; $\overline{j} = 30$

$\Delta\theta$. In the quantum mechanical model, however, the peak of the curve is rarely exactly $\Delta\theta = 0$. Only a few transitions allow a $\Delta\theta$ of exactly 0. This behavior is especially noticeable when j and j' are small or when Δj is very large.

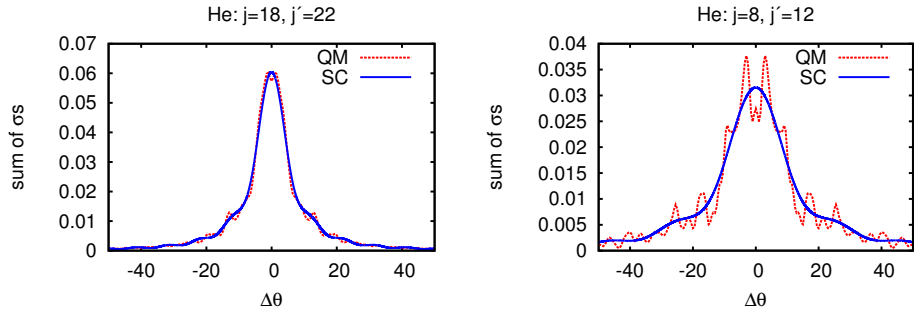

Figure 11: Cross sectional distribution vs. $\Delta\theta$, averaged over all collisions; $\overline{j} = 20$ (left); $\overline{j} = 10$ (right)

4.6 Results: $m \to m'$

Filtering the quantum mechanical data by m and m' and smoothing with a spline gives Figure 12. The curves do not all peak where $m = m'$, unlike

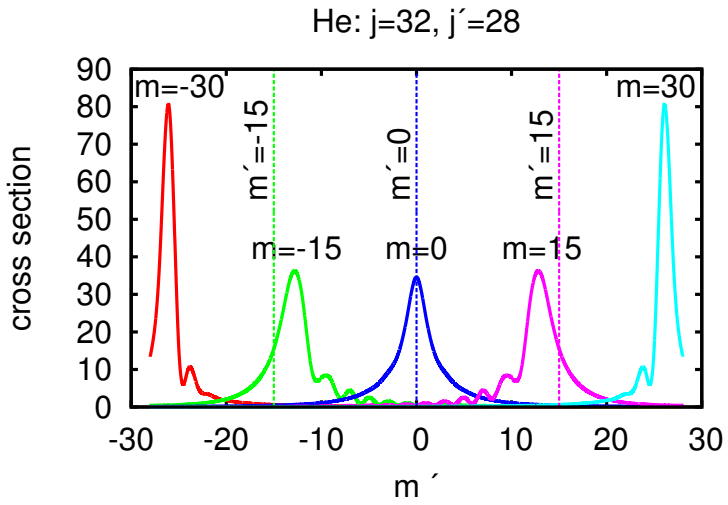

Figure 12: Cross sectional distribution vs. m' for the indicated initial quantum number m. Vertical lines represent where $\Delta m = 0$

the $\theta \to \theta'$ distributions (Figure 9). This is to be expected. j and j' change, and if θ is approximately constant, then m must change in such a way that $\Delta\theta$ is close to zero. Both the semiclassical and quantum mechanical models exhibit this behavior. The semiclassical model does not have the

same oscillations that the quantum mechanical model has for $m \neq 0$ curves, but it appears to average over those oscillations, which is expected for a semiclassical approximation to a quantum mechanical system.

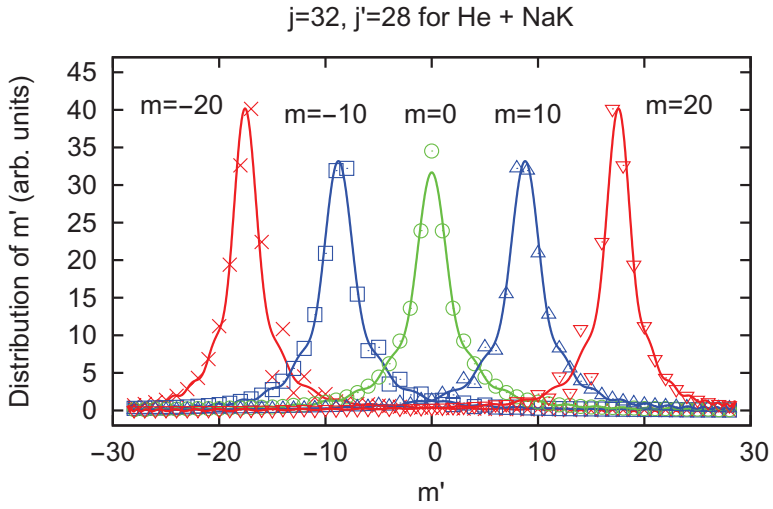

Figure 13: Cross sectional distribution vs. m' for the indicated initial quantum number m. The lines are the semiclassical calculations and the points are the quantum mechanical results.

4.7 Conclusions for Cross Section Analysis

Figure 13 illustrates the good agreement between semiclassical and quantum mechanical calculations for $m \rightarrow m'$ transitions. θ tends to be conserved, which is consistent with other research in this field [5]. m tends to change in such a way that $\Delta\theta$ is small. This means the orientation tends to be preserved during collisions of NaK with He and Ar. The physical interpretation of the vector model offers deeper understanding of this behavior by modeling both $\boldsymbol{j}$ and $\boldsymbol{j'}$ vectors. By extending the vector model from one $\boldsymbol{j}$ vector to account for both j and j', as well as modeling the changes in m and θ, it has been shown that, for a particular j to j' transition, m will change in a certain way to approximately preserve θ. The semiclassical model is a good approximation for the quantum mechanical model, especially when j and j' are large.

5 Acknowledgments

A.C.T. acknowledges support by NSF under the REU program at Lehigh University Physics Department and Grant Nos. PHY-0968898 and PHY-1403060. Computational facilities at the Texas Advanced Computing Center (TACC) used for this research were supported by NSF from XSEDE resources provided by the XSEDE Science Gateways Program. The author acknowledges stimulating conversations with J. Huennekens, Teri Price, and Kara Richter as well as their patient hospitality. The author would like to thank M. V. McSwain for logistical support. The author would like to thank A. P. Hickman for his explanations and mentorship.

References

[1] S. Magnier, M. Aubert-Frécon, and Ph. Millié, "Potential Energies, Permanent and Transition Dipole Moments for Numerous Electronic Excited States of NaK", J. Mol. Spectrosc. **200**, 96–103 (2000).

[2] J. A. Jones, Ph.D. thesis, Lehigh University, 2015.

[3] C. M. Wolfe, S. Ashman, J. Bai, B. Beser, E. H. Ahmed, A. M. Lyyra, and J. Huennekens, "Collisional transfer of population and orientation in NaK", J. Chem. Phys. **134**, 174301 (17 pages) (2011).

[4] R. F. Malenda, T. J. Price, J. Stevens*, S. L. Uppalapati*, A. Fragale*, P. M. Weiser, A. Kuczala*, D. Talbi, and A. P. Hickman, "Theoretical calculations of rotationally inelastic collisions of He with NaK($A\,^1\Sigma^+$): Transfer of population, orientation, and alignment", J. Chem. Phys. **142**, 224301 (12 pages) (2015).

[5] M. H. Alexander and S. L. Davis, "M dependence in rotationally inelastic scattering in cell experiments: Implications of an irreducible tensor expansion for molecules in $^1\Sigma$ electronic states", J. Chem. Phys. **78**, 6754–6762 (1983).

[6] J. Derouard, "Reorientation, polarization and scaling laws in rotational transfer experiments", Chem. Phys. **84**, 181–192 (1984).

[7] J. Huennekens (personal communication).

[8] T. Price (personal communication).

[9] A. P. Hickman, "Semiclassical Model for the Distribution of Polar Angles after Rotationally Inelastic Collisions in a Cell Environment", A. P. Hickman (2015).